Dual wavelength magneto-optical imaging of magnetic thin films

Thomas von Hofe, Necdet Onur Urs, Babak Mozooni, Thomas Jansen, Christine Kirchhof, Daniel E. Bürgler, Eckhard Quandt, and Jeffrey McCord

Citation: Applied Physics Letters **103**, 142410 (2013); doi: 10.1063/1.4824426
View online: http://dx.doi.org/10.1063/1.4824426
View Table of Contents: http://scitation.aip.org/content/aip/journal/apl/103/14?ver=pdfcov
Published by the AIP Publishing

Dual wavelength magneto-optical imaging of magnetic thin films

Thomas von Hofe,[1] Necdet Onur Urs,[1] Babak Mozooni,[1] Thomas Jansen,[2] Christine Kirchhof,[1] Daniel E. Bürgler,[2] Eckhard Quandt,[1] and Jeffrey McCord[1,a)]
[1]*Institute for Materials Science, University of Kiel, Kaiserstraße 2, 24143 Kiel, Germany*
[2]*Peter Grünberg Institut, Electronic Properties (PGI-6), Forschungszentrum Jülich, 52425 Jülich, Germany*

(Received 10 August 2013; accepted 19 September 2013; published online 3 October 2013)

A magneto-optical imaging approach for the simultaneous imaging of multiple magnetization components is demonstrated. The method is applied to investigate complex magnetization reversal processes in single crystal iron and patterned amorphous magnetostrictive ferromagnetic structures. The use of a splitted optical illumination and observation path allows for the direct extraction of different complementary magnetic information. Real-time in-plane vector magnetization imaging reveals complicated domain arrangement processes in magnetostrictive films due to locally varying stress induced magnetic anisotropy. Magnetic domain features concealed by standard domain imaging techniques are directly exposed. © *2013 AIP Publishing LLC*.
[http://dx.doi.org/10.1063/1.4824426]

The imaging of magnetic domains in magnetic materials is essential to obtain an understanding of the underlying mechanisms of magnetization reversal and the related processes in micro- or nanoscale magnetic devices,[1] e.g., spintronic applications. This promotes further development in domain imaging techniques. Despite recent years' advances, mainly in improving lateral and temporal resolution, the continuous imaging of the vector nature of magnetization cannot be performed. Yet, integral magnetic vector information can be extracted from magnetization loop measurements. Vector magnetometry can be performed for instance by means of vibrating sample magnetometry[2–4] and by magneto-optics,[5–8] from which, however, no information on the domain state can be extracted.

Essentially, vectorial magnetic domain observation is merely possible by imaging methods that provide a signal being proportional to the magnetization **M** of the observed magnetic materials and offer as well the possibility of separating different components of **M** individually. Applied vectorial domain imaging methods, like scanning electron microscopy with polarization analysis,[9–12] differential phase contrast Lorentz transmission electron microscopy,[13,14] electron holography,[15] or X-ray microscopy[16] require a rather long exposure time of up to several minutes. The process of obtaining magnetic vector information by magneto-optics[17–19] involves multiple calibration images that must be taken before and after the imaging of the magnetization pattern of interest. In particular, the scheme is restricted to static magnetization patterns, as the same magnetization distribution has to be imaged subsequently under different imaging conditions, from which only a single vector image of an individual stationary domain structure can be constructed. For the case of the associated scanning Kerr microscopy, vector components of **M** can be extracted, however, likewise with a rather long integration and scanning time. Similar restrictions exist for the (scanning) type domain imaging techniques mentioned above. Methods that allow for the real-time investigation of local magnetization directions, providing at least partial vector information of magnetic domains or domain walls, do not exist.

In this letter, real-time vector imaging of the spatial variation of **M** using dual wavelength magneto-optical microscopy is demonstrated for the investigation of magnetic thin films. First, the applicability of the method to extract magnetization vector data in real-time is proven. Second, we investigate the magnetization structure in high magnetostrictive films as used for magnetoelectric composites that display a variety of changing complex magnetic structures due to a lateral stress induced distribution of effective magnetic anisotropy.

The employed technique for the investigation of magnetic domain structures is based on the merging of two imaging paths with different wavelengths in the microscope. The overall experimental arrangement is sketched in Fig. 1. For the shown implementation of the method red ($\lambda = 630$ nm) and blue ($\lambda = 490$ nm) light from high power light emitting diodes (LED) with >1 W of collimated output power are used for illumination. The LEDs are coupled into the

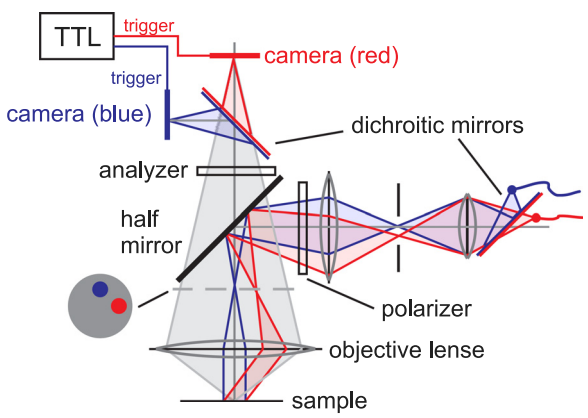

FIG. 1. Microscope illumination ray path for the complementary imaging of magnetic domain structures. Each of the individual illumination paths follows the Köhler-type illumination principle. Unification and divergence of the light paths are achieved by dichroitic mirrors.

a)Electronic mail: jmc@tf.uni-kiel.de

illumination path through optical fibers, by that allowing an individual positioning of the fiber outputs in the microscope objective's back focal image plane. In this way, an independent adjustment of the illumination conditions for both light sources is achieved. By focussing and positioning the red and blue LED fiber outputs accordingly (Fig. 1) oblique and orthogonally aligned planes of incidence are achieved. An imaging scheme using s- and p-mode longitudinal Kerr sensitivity is sketched in Fig. 2(a). The imaging beams are united into the illumination light path through a wavelength sensitive dichroitic mirror, by which two separate and independent imaging conditions can be achieved. In the observation light path, the reflected light is redivided into red and blue beams directed individually to two high sensitivity microscope cameras. Image exposure of the two cameras is synchronized by an external trigger (TTL) signal, ensuring concurrent image acquisition for the two imaging conditions of choice. Both imaging paths share the optical polarizing elements.

Two complementary domain images of an epitaxial Fe film, displaying both longitudinal magnetic information of a single magnetic configuration, are displayed in Fig. 2(b). The images prove the general feasibility of dual wavelength domain imaging technique.

The calibration of the individual magneto-optical sensitivity directions is performed as described in Ref. 19. However, only a single calibration procedure is needed for the extraction of the magnetic vector information from multiple sequentially obtained image pairs. Results from the dual wavelength vectorial domain analysis of moving domains in a single crystal iron film are displayed in Fig. 3. The evaluated quantitative information of the magnetization distribution as well as the individual components of **M** are displayed. The calculated distribution of **M** is in accordance with the known easy axes of anisotropy in the single crystal Fe film. The angular error of the determined magnetic directions is almost negligible, as seen from the minimal contrast between the magnetic domains with **M** aligned antiparallel to each other, but orthogonal to the displayed magnetization components in Figs. 3(b) and 3(c). Computationally rotating

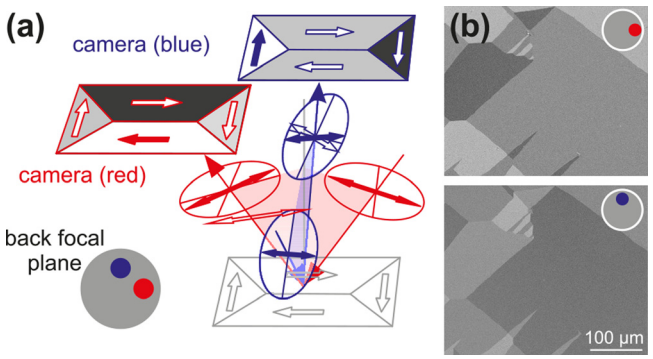

FIG. 2. (a) Simultaneous measurement of the longitudinal Kerr effect in the s- and p-mode with the red and blue, respectively, microscope ray paths. (b) Concurrently obtained Kerr images of a single crystal iron film with orthogonal sensitivity directions. The corresponding illumination arrangements in the back focal plane of the objective are indicated. 32 images of the static domain state were acquired simultaneously and averaged in order to improve the signal-to-noise ratio in the domain images. (Sample: GaAs/Fe(1 nm)/Ag (150 nm)/Fe(50 nm)/ZnS).

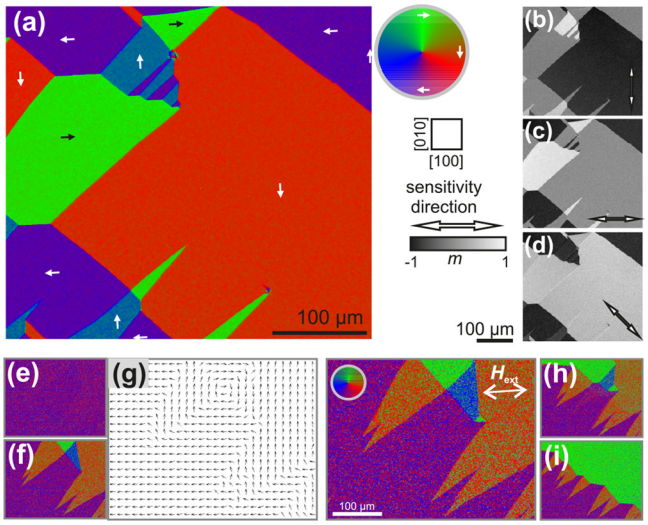

FIG. 3. (a) Quantitative magneto-optical image from the magnetic structure of Fig. 2(b). The angular distribution of **M** is color coded as indicated in the inset. Extracted magnetization components along (b) the y-direction, (c) the x-direction, and (d) the diagonal direction. The axes of the displayed components of **M** are indicated in (b)–(d) by arrows. The (100) easy axis directions of the magnetic thin film are indicated. (e)–(i) Magnetic reversal in the Fe thin film. The color coded angular magnetization distributions and an exemplary magnetic vector plot are shown (see supplementary material[20]). The orientation of the external magnetic field H_{ext} is indicated. (Sample: GaAs/Fe(1 nm)/Ag (150 nm)/Fe(50 nm)/ZnS).

the effective sensitivity axis to lie at 45° relative to the easy axes of magnetization confirms the statement (Fig. 3(d)). 180° and 90° domain wall contrasts, respectively, become visible in the images. Using the same procedure, quantitative domain information of constantly realigning domains was obtained. Some extracted magnetization vector information is displayed in Figs. 3(e)–3(i). No image averaging for noise reduction is performed. The exposure time of the individual single-shot domain image pairs obtained in real-time is 0.05 s. Starting from the saturated state (Fig. 3(e)) the magnetization reversal process occurs by combined 180° and 90° domain wall motion. After the instantaneous nucleation of 90° spike domains and a magnetic vortex structure (Figs. 3(f) and 3(g)), the vortex structure is expanding to a different domain wall arrangement, including a central 180° wall (Fig. 3(h)). Subsequently, the reversal process is accompanied by continuous motion of a 180° or 90° domain wall network (Fig. 3(i)). Again, the obtained magnetic vector data, an example of which is displayed in Fig. 3(g), is in agreement with the magnetocrystalline cubic anisotropy distribution of the thin film.

The magnetic reversal in an amorphous ferromagnetic FeCoBSi layer as used for magnetoelectric composite AlN/FeCoBSi sensor structures[21,22] is investigated next. Most importantly, the alignment and distribution of magnetic anisotropy is of significance in order to obtain a defined magnetoelectric response signal.[22] The effective anisotropy distribution in the structured films will directly influence the exhibited magnetic domain distribution. The control of the magnetic domain rearrangement processes under the application of varying magnetic fields is of essential importance in order to understand and minimize the origin of magnetically induced (Barkhausen) noise.[23] For the highly magnetostrictive

alloy the domain behavior is strongly determined by local stress effects as will be evidenced next.

Complementary domain images sequentially obtained for two orthogonal magneto-optical sensitivity directions and various magnetic field values are displayed in Fig. 4. The nominal anisotropy axis (EA) of the system is vertical in Fig. 4. The magnetic field is aligned perpendicular to the nominal EA of the system and parallel to specimen's edge at the bottom. Starting from high magnetic fields, antiparallel aligned domains form with **M** oriented close, but slightly tilted to the initial EA form. However, the domains are not reaching the structure's edge at the bottom and closure domains form inside the magnetic structure. Concurrent with reduction of the field amplitude, the domains penetrate from the center portion of the film towards the edges (dotted line in Fig. 4). Yet, the partially dagger-shaped closure domains never reach the sample's edge. The magnetization at the edge stays aligned with the sample's edge, indicating an alignment of effective magnetic anisotropy parallel to sample's edge in the region close to the edge orthogonal to the initial anisotropy direction. Similar domain structures are discussed in anisotropy patterned magnetic thin films or magnetic film structures with stress relaxation at the edges.[6] The origin is tensile stress in the films, which then in connection with edge relaxation effects leads to a total realignment of magnetic anisotropy direction.

With the transformation process, the magnetic Bloch line first visible in the bottom image of Fig. 4(e) (see arrow) starts to move to the edge of the sample, and then in the reversing field before switching (Fig. 4(h)) back inside the sample. With reversing the magnetic field the magnetization at the edge switches instantaneously (from Figs. 4(i) and 4(j)) along the field direction. With increasing field amplitude the inner domain walls pull back from the edges again.

The color-coded magnetization distribution, the calculated magnetic vector plot, and the complementary domain images before, during, and after the magnetic switching event are displayed in detail in Figs. 5(a)–5(h). The main deviation in the domain structure between the two magnetic states lies in the switching of magnetization by nearly 180° close to the sample's edge, clearly visible in the (red) horizontal sensitivity direction. However, with the reversal the bended domain wall structure in the bulk portion of the sample changes position, one type of closure domains and the connected 180° domain walls annihilate, rearranging to form a closure domain at the neighboring domain. Likewise the dagger-shaped spike domain switches position. The domain structure apart from the edge, visible in the (blue) vertical sensitivity images, seems to be uninfluenced, but the reversal of magnetization at the edges also influences the magnetization inside the sample. The difference Δ between the magnetic states extracted for both sensitivity directions is displayed in Figs. 5(i) and 5(j). Due to the reorganization of the closure domain states with the switching event, the reversal is accompanied by 180° domain wall motion in the neighboring regions. Yet, the overall magnetization alignment within the domain in the central portion of the film stays constant, no additional change of magnetic contrast that would be related to the rotation of magnetization inside the domain is found.

Overall, the magnetic reversal inside the sample is accompanied by rotation of magnetization and domain wall motion. Also internal changes in the wall structure occur. Only by visualizing both magnetization components simultaneously, the magnetization distribution, including domain and domain wall effects, can be determined accurately and the mixed hard and easy axis magnetic reversal behavior and its connection is identified undoubtedly.

In conclusion, the addition of direct real-time vector imaging to magneto-optical Kerr microscopy is demonstrated. The technique is applied to investigate complex magnetization reversal in magnetic film structures. Using

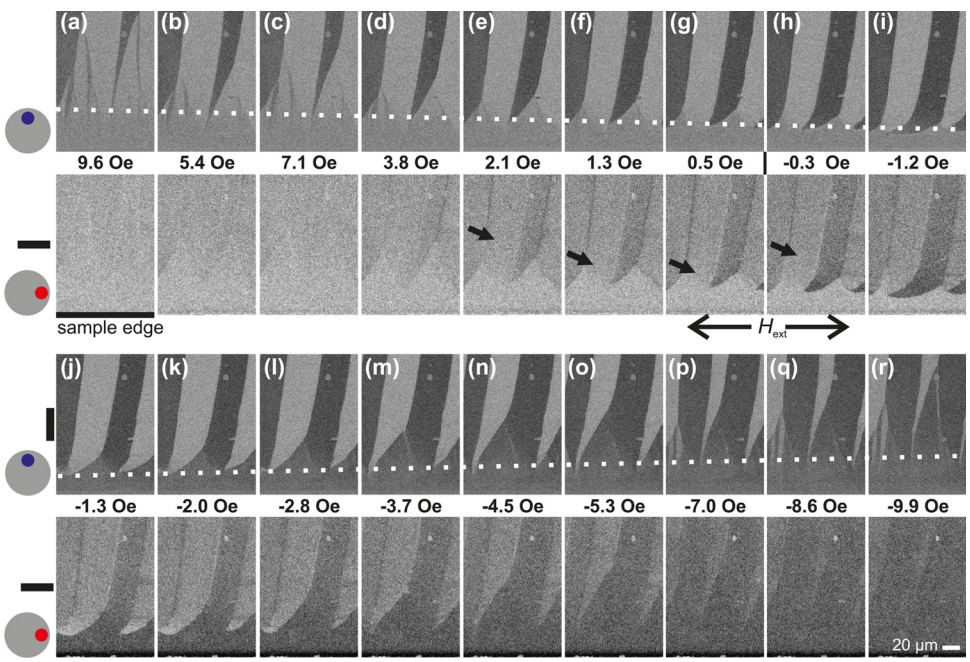

FIG. 4. Magnetization reversal in the ferromagnetic FeCoBSi layer (see supplementary material[20]). (a)–(r) Complementary domain images with orthogonal sensitivity direction. The edge of the sample is located on the bottom of the images. The orientation and amplitude of the applied magnetic field H_{ext} is indicated. The exposure time of the individual domain images is 0.05 s. (Sample: $Si/SiO_2/Ta(10\,nm)/(Fe_{90}Co_{10})_{78}B_{10}Si_{12}(2000\,nm)/Ta(5\,nm)$).

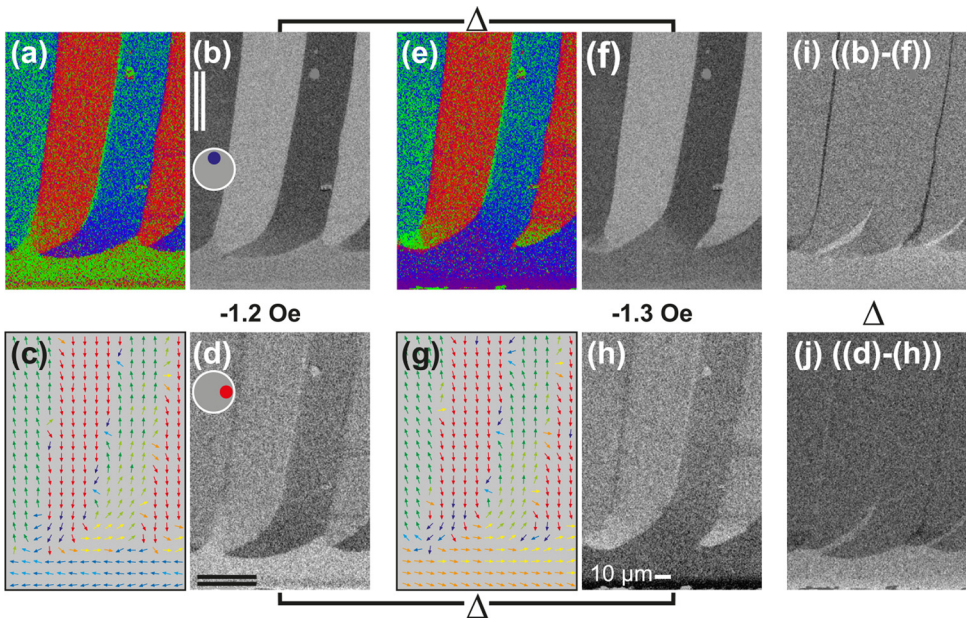

FIG. 5. Magnetization reversal in the ferromagnetic FeCoBSi layer around H_c. (a) and (e) Color-coded angular distributions of **M** before and after the magnetic switching event. (c) and (g) Display the corresponding magnetic vector plots. (b), (d) and (f), (h) Show the complementary images with orthogonal sensitivity directions. In (i) and (j) the change (Δ) of magnetization as imaged for the different sensitivity directions during switching is displayed. The edge of the sample structure is on the bottom. The amplitude of H_{ext} is indicated. (Sample: $Si/SiO_2/Ta(10\,nm)/(Fe_{90}Co_{10})_{78}B_{10}Si_{12}(2000\,nm)/Ta(5\,nm)$).

two imaging paths, domain images with different vector components are recorded simultaneously. The spatial variation of the magnetization vector is extracted directly and in real-time. In principle, the method is not limited to the shown quantitative domain imaging. Additional embodiments include the adaption to methods that rely on the combination of different imaging conditions. This includes layer selective magnetic domain imaging as well as the separation of in-plane and out-of-plane magnetization components (i.e., separation of longitudinal and polar Kerr contrast) in film structures with out-of-plane and in-plane magnetization components. Moreover, the method can be applied to time-resolved stroboscopic and single shot imaging schemes using pulsed-laser illumination sources. With the addition of real-time multiple component imaging to full field magneto-optical Kerr microscopy the technique will continue to be of great importance for the investigation of fundamental and applied aspects of magnetization domain processes in magnetic materials. Magneto-optical imaging is taken to the next level.

Funding through the German Research Council Heisenberg Programme (DFG, MC9-10/1) and the Collaborative Research Center SFB 855 is highly appreciated.

[1]A. Hubert and R. Schäfer, *Magnetic Domains - The Analysis of Magnetic Microstructures* (Springer, Berlin, 1998).
[2]T. Bolhuis, L. Abelmann, J. C. Lodder, and E. O. Samwel, J. Magn. Magn. Mater. **193**, 332 (1999).
[3]S. U. Jen and J. Y. Lee, J. Magn. Magn. Mater. **271**, 237 (2004).
[4]P. Stamenov and J. M. D. Coey, J. Appl. Phys. **99**, 08D912 (2006).
[5]H. Ohldag, N. B. Weber, F. U. Hillebrecht, and E. Kisker, J. Appl. Phys. **91**, 2228 (2002).
[6]J. McCord, J. Appl. Phys. **95**, 6855 (2004).
[7]P. S. Keatley, V. V. Kruglyak, R. J. Hicken, J. R. Childress, and J. A. Katine, J. Magn. Magn. Mater. **306**, 298 (2006).
[8]A. Westphalen, M. S. Lee, A. Remhof, and H. Zabel, Rev. Sci. Instrum. **78**, 121301 (2007).
[9]M. R. Scheinfein, J. Unguris, J. L. Blue, K. J. Coakley, D. T. Pierce, R. J. Celotta, and P. J. Ryan, Phys. Rev. B **43**, 3395 (1991).
[10]A. Gavrin and J. Unguris, J. Magn. Magn. Mater. **213**, 95 (2000).
[11]H. P. Oepen, G. Steierl, and J. Kirschner, J. Vac. Sci. Technol. B **20**, 2535 (2002).
[12]D. T. Pierce, J. Appl. Phys. **109**, 07E106 (2011).
[13]J. N. Chapman, I. R. McFadyen, and S. McVitie, IEEE Trans. Magn. **26**, 1506 (1990).
[14]M. C. Hickey, D. T. Ngo, S. Lepadatu, D. Atkinson, D. McGrouther, S. McVitie, and C. H. Marrows, Appl. Phys. Lett. **97**, 202505 (2010).
[15]M. R. McCartney and Y. M. Zhu, J. Appl. Phys. **83**, 6414 (1998).
[16]S. K. Kim, J. B. Kortright, and S. C. Shin, Appl. Phys. Lett. **78**, 2742 (2001).
[17]W. Rave, R. Schäfer, and A. Hubert, J. Magn. Magn. Mater. **65**, 7 (1987).
[18]W. Rave and A. Hubert, IEEE Trans. Magn. **26**, 2813 (1990).
[19]W. Rave, P. Reichel, H. Brendel, M. Leicht, J. McCord, and A. Hubert, IEEE Trans. Magn. **29**, 2551 (1993).
[20]See supplementary material at http://dx.doi.org/10.1063/1.4824426 for a movie of the complete reversal process.
[21]H. Greve, E. Woltermann, R. Jahns, S. Marauska, B. Wagner, R. Knöchel, M. Wuttig, and E. Quandt, Appl. Phys. Lett. **97**, 152503 (2010).
[22]H. Greve, E. Woltermann, H. J. Quenzer, B. Wagner, and E. Quandt, Appl. Phys. Lett. **96**, 182501 (2010).
[23]R. Jahns, H. Greve, E. Woltermann, E. Quandt, and R. H. Knöchel, IEEE Trans. Instrum. Meas. **60**, 2995 (2011).